

UC Merced

UC Merced Previously Published Works

Title

SUGT1 controls susceptibility to HIV-1 infection by stabilizing microtubule plus-ends

Permalink

<https://escholarship.org/uc/item/0sb8r3vm>

Journal

Cell Death & Differentiation, 27(12)

ISSN

1350-9047

Authors

Allouch, Awatef
Di Primio, Cristina
Paoletti, Audrey
et al.

Publication Date

2020-12-01

DOI

10.1038/s41418-020-0573-5

Peer reviewed



SUGT1 controls susceptibility to HIV-1 infection by stabilizing microtubule plus-ends

Awatef Allouch^{1,2,3,4} · Cristina Di Primio⁵ · Audrey Paoletti^{1,2,3,4} · Gabrielle Lê-Bury^{6,7,8} · Frédéric Subra⁹ · Valentina Quercioli⁵ · Roberta Nardacci¹⁰ · Annie David¹¹ · H la Saïdi¹² · Anna Cereseto¹³ · David M. Ojcus^{14,15} · Guillaume Montagnac¹⁶ · Florence Niedergang^{6,7,8} · Gianfranco Pancino¹¹ · Asier Saez-Cirion¹¹ · Mauro Piacentini^{10,17} · Marie-Lise Gougeon¹² · Guido Kroemer^{8,18,19,20,21,22} · Jean-Luc Perfettini^{1,2,3,4,14}

Received: 4 September 2019 / Revised: 27 May 2020 / Accepted: 29 May 2020 / Published online: 8 June 2020
  The Author(s), under exclusive licence to ADMC Associazione Differenziamento e Morte Cellulare 2020

Abstract

Understanding the viral–host cell interface during HIV-1 infection is a prerequisite for the development of innovative antiviral therapies. Here we show that the suppressor of G2 allele of *skp1* (SUGT1) is a permissive factor for human immunodeficiency virus (HIV)-1 infection. Expression of SUGT1 increases in infected cells on human brain sections and in permissive host cells. We found that SUGT1 determines the permissiveness to infection of lymphocytes and macrophages by modulating the nuclear import of the viral genome. More importantly, SUGT1 stabilizes the microtubule plus-ends (+MTs) of host cells (through the modulation of microtubule acetylation and the formation of end-binding protein 1 (EB1) comets). This effect on microtubules favors HIV-1 retrograde trafficking and replication. SUGT1 depletion impairs the replication of HIV-1 patient primary isolates and mutant virus that is resistant to raltegravir antiretroviral agent. Altogether our results identify SUGT1 as a cellular factor involved in the post-entry steps of HIV-1 infection that may be targeted for new therapeutic approaches.

Introduction

The design of novel therapeutic antiviral approaches to inhibit the replication of drug-resistant HIV-1 strains assumes a detailed understanding of the cellular factors that promote viral replication steps. Independently from the process of viral entry into target cells, HIV-1 rapidly traffics on stable microtubules, which are characterized by high acetylation levels of α -tubulin at lysine 40 (K40), to reach the nucleus and integrate in the human genome [1, 2]. A large list of microtubule-binding proteins is involved in HIV-1 uncoating and stabilization of viral complexes to accomplish reverse transcription and cytoplasmic viral trafficking (reviewed in ref. [3]). Since the suppressor of G2

allele of *S-phase kinase-associated protein 1* (*skp1*) (SUGT1) protein can attach proteins onto microtubules [4–8], we investigated the role of SUGT1 in the early cellular response to HIV-1 infection. Initially described as a co-chaperone of heat shock protein 90, SUGT1 is involved in the innate immune response in plants and mammals [9] through the activation of nucleotide-binding domain and leucine-rich repeat containing proteins. Here, we showed that SUGT1 is a permissive cellular factor for HIV-1 infection. We demonstrated that SUGT1 promotes HIV-1 reverse transcription and nuclear import through the stabilization of microtubule plus-ends that are required for efficient HIV-1 cytoplasmic trafficking. Altogether, our results identify and characterize SUGT1 as a cellular factor that is essential for early steps of HIV-1 infection.

Edited by G. Melino

Supplementary information The online version of this article (<https://doi.org/10.1038/s41418-020-0573-5>) contains supplementary material, which is available to authorized users.

✉ Jean-Luc Perfettini
perfettini@orange.fr

Extended author information available on the last page of the article

Materials and methods

Cells and reagents

Buffy coats from healthy donors were obtained through the French blood bank (Etablissement Fran ais du sang (EFS)) as part of EFS-INSERM Convention in accordance with

French law. Monocytes were obtained from buffy coats and differentiated into macrophages as previously described [10]. Monocytes were first separated from peripheral blood mononuclear cells (PBMCs) by adherence to the plastic and then cultured for 6–7 days in hydrophobic Teflon dishes (Lumox; Duthsher) in macrophages medium (Roswell Park Memorial Institute (RPMI) 1640 medium supplemented with 200 mM L-glutamine, 100 U of penicillin, 100 µg streptomycin, 10 mM HEPES, 10 mM sodium pyruvate, 50 µM β-mercaptoethanol, 1% minimum essential medium vitamins, and 1% nonessential amino acids) containing 15% of heat-inactivated human serum AB. Monocyte-derived macrophages (MDMs) were then harvested and suspended in macrophage medium containing 10% of heat-inactivated fetal bovine serum (FBS). Flow cytometry analysis using anti-CD14 (eBioscience, #12-0149-42), anti-CD11b (Pharmingen, #557918), anti-CD71 (Pharmingen, #555537), anti-CD163 (Pharmingen, #562669), and anti-CD206 (Pharmingen, #551135) antibodies revealed that 91–96% of MDMs expressed both differentiation (CD14, CD11b, and CD71) and M2 macrophage (CD163 and CD206) markers. The purity of MDMs was also controlled by the negative staining for anti-CD56 (#560916) (NK cells), anti-CD3 (#555339) (T cells), and anti-CD20 (#559776) (B cells) antibodies. All antibodies used were from Pharmingen. The primary blood T-lymphocytes (PBLs) were isolated from the non-adherent PBMCs fraction using the T cells negative selection kit (STEM CELL). Lymphocytes obtained by this method were 90–97% CD3 expressing T cells and were cultured in RPMI medium containing 10% FBS. T lymphocytes (5×10^6 /ml) were stimulated by phytohemagglutinin (5 µg/ml) for 72 h in medium containing IL2 (25 units/ml) (Roche), suspended at 10^6 /ml in IL2 medium and cultured for additional 2 days for Western blot (WB) analysis of SUGT1 expression level and HIV-1 infection, and 3 days for SUGT1-mediated siRNA silencing. Activation of T cells was determined with anti-CD25 (BD Pharmingen, #560987) and anti-CD69 (BD Pharmingen, #557049) antibodies by flow cytometry. HeLa CD4⁺CXCR4⁺, HEK293T and U2OS cell lines were obtained from GK (Gustave Roussy Cancer Campus, France) and HeLa cells were obtained from GM (Gustave Roussy Cancer Campus, France). These cell lines were cultured in Dulbecco's modified Eagle's medium-Glutamax supplemented with 10% FBS and 100 UI/ml penicillin-streptomycin. All cell lines used were mycoplasma-free.

Human autopsies

Human autopsies from frontal cortex were obtained in accordance with Italian and EU legislations, after approval by the Institutional Review Board of the Italian Lazzaro Spallanzani National Institute for Infectious Disease (Ethics

Committee approval number 40/2006). Postmortem frontal cortex sections were obtained from three uninfected individuals and nine individuals with HIV-1-associated dementia (all men, mean age 36 years; the median values of HIV-1 viral load was $4.5 \pm 0.6 \log_{10}$ cp/ml and <500 CD4 T cells/ml). All individuals consented to the research use of their frontal cortex brain autopsies at postmortem.

RNA interference

The siGenome smart small interfering RNAs (siRNAs) were all purchased from Dharmacon. The siRNA against SUGT1 (siSUGT1) gene is composed a pool of four siRNAs. The indicated siRNAs have the following sequences: siSUGT1: (1) 5'-GAUCAAGAAUGUUCAGAAG-3', (2) 5'-GAACUUCUUAUCCUAUAA-3', (3) 5'-GCAAAGAAGUCUCUAGAAC-3', and (4) 5'-GAACCUAUAUCCAUCAUCA-3'. The control siRNA is a pool of four on target plus non-targeting siRNAs (siCo.). The single siSUGT1 (siSUGT1-1) used for HeLa CD4⁺CXCR4⁺ cell lines was previously described [9]: 5'AAGGCUUUGAACAGAAACCA-3' and the corresponding control siRNA: 5'-UUCAAUAAUUCUUGAGGU-3' were both synthesized from Sigma. Macrophage silencing was previously described with some modifications [10]. Briefly, MDMs (1×10^6 /ml of macrophages medium + 10% FBS) were allowed to be attached at 37 °C for 2 h prior to siRNAs transfection, which was performed with the INTERFERin (Polyplus Transfection). siSUGT1 or siCo. (8 µl from 20 µM stock solution) were pre-diluted in 1 ml of Opti-MEM in which 40 µl of INTERFERin were added and the transfection mix was incubated at room temperature for 10 min. The transfection mix (500 µl) was added to 10^6 for 50 nM final siRNA concentration. MDMs were then incubated at 37 °C for 24 h and the medium was replaced with fresh macrophage medium supplemented with 10% FBS for additional 48 h prior infections. Activated lymphocytes were suspended in RPMI-IL2 medium (10^7 PBLs/ml) to which 125 µl of the transfection mix containing: 1 ml Opti-MEM, 20 µl INTERFERin, and 4 µl of siRNA from 20 µM stock solution were added for 6.25 nM final siRNA concentration. After 6 h incubation, PBLs were suspended in fresh RPMI-IL2 medium (5×10^6 cells/ml) and cultured for additional 72 h prior HIV-1 infection. For HeLa, HEK293T and U2OS cells, the final siRNAs concentrations were at 10 pmol transfected with RNAi MAX (Promega) following the manufacturer's instructions. Cell lysates were assayed for protein expression by Western blot to determine the knockdown efficiency at infection at 72 h for MDMs, PBLs, and HEK293T cells and 48 h for U2OS and HeLa cells post silencing. Cell viability and cytotoxicity following silencing were determined by WST-1 assay, MTT assay, or the lactate dehydrogenase release assay (all from Sigma).

Plasmid transfections

HEK293T cells (2.5×10^6) were transfected with 5 μg pcDNA3-HA-tagged integrase (HA-IN) or pcDNA3-HA (HA) empty vector using Fugene (Promega). After 48 h of transfection, cells were harvested for co-immunoprecipitation assays. U2OS cells (5×10^3) were silenced by siSUGT1 (20 nM) and siControl siRNAs using RNAi max (Qiagen) and at 24 h later were transfected with 0.5 μg pcDNA3-HA-IN or pcDNA3-HA for 24 h. For bulk SUGT1 overexpression, HEK293T cells (10^5) were transfected with 0.75 μg of pCMV-SPORT6-SUGT1 (SUGT1) or pEGFP-N1-GFP control plasmid using Fugene (Promega). After 48 h of transfection, cells were infected and analyzed by western blots. For GFP-based flow cytometry sorting, HEK293T cells (10^5) were transfected with 0.75 μg of pRLL-EF1-SUGT1-PGK-GFP using Fugene (Promega). After 48 h of transfection, the GFP⁻ and GFP⁺ cells were sorted by FACS, kept for further 24 h prior western blot analysis and infections.

Viral constructs, viruses, lentiviral vectors, and in vitro infections and transductions

Single round HIV-1 infections were performed with the VSV-G envelop pseudotyped viruses: HIV-1 $_{\Delta\text{EnvNL4-3-Luc}}$ and HIV-1 $_{\Delta\text{EnvNL4-3-IND64E}}$ that contain luciferase as a reporter gene, HIV-1 $_{\Delta\text{EnvNL4-3-GFP-Vpr}}$ that incorporates GFP-Vpr molecules or with HIV-1 $_{\text{CMV-GFP-I-SCEI}}$, HIV-1 $_{\Delta\text{EnvNL4-3-Luc}}$, HIV-1 $_{\Delta\text{EnvNL4-3-IND64E}}$, and HIV-1 $_{\Delta\text{EnvNL4-3-GFP}}$ were obtained through the co-transfection of 3×10^6 HEK293T cells with 20 μg pNL4.3-Luc Nef-Env-, pD64E, both from NIH AIDS research reagents and 5 μg pMD2-VSV-G expression vectors following calcium phosphate transfection procedure (Promega). HIV-1 $_{\Delta\text{EnvNL4-3-GFP-Vpr}}$ was obtained through the transfection of 3×10^6 HEK293T cells with 10 μg pNL4.3-Luc Nef-Env- (NIH AIDS research reagents), 2.5 μg pGFP-Vpr, and 2.5 μg pMD2-VSV-G expression vectors using Fugene (Promega) following manufacturer's instructions. For HIV-1 $_{\Delta\text{EnvNL4-3-GFP-Vpr}}$ (VSV-G) supernatants harvest at 48 h post transfection and were concentrated by 2 h of ultracentrifugation in 20% (wt/vol) sucrose cushion. VSV-G-pseudotyped HIV-1 $_{\text{CMV-GFP-I-SCEI}}$ was obtained as previously described [11]. Briefly, HIV-1 $_{\text{CMV-GFP-I-SCEI}}$ virions were produced by transient transfection of 3×10^6 HEK293T cells by using 150 nM polyethylenimine (PEI) reagent (Sigma) with 20 μg of pHR-CMVGFP-I-SceI plasmid, 15 μg of p Δ 8.91 packaging, and 5 μg of pVSV-G envelope expressing plasmid. Supernatants were collected after 48 h, filtered through a 0.45 μm pore size filter and then concentrated by ultracentrifugation in 20% (wt/vol) sucrose cushion. HIV-1 $_{\text{IN-EGFP}}$ virions [12] were produced by transfecting 3×10^6 HEK293T cells by using 150 nM PEI reagent (Sigma) with

6 μg of pVpr-IN-EGFP, 6 μg of pD64E, and 1 μg of pVSV-G. Supernatants were collected after 48 h, filtered through a 0.45 μm pore size filter and then concentrated by ultracentrifugation. For replication competent viruses, HIV-1 $_{\text{NL4-3}}$ and HIV-1 $_{\text{AD8}}$ were obtained through the transfection of 3×10^6 HEK293T cells with 15 μg of pHIV-1-NL4-3 and pHIV-1-AD8 following calcium phosphate transfection protocol (Promega). HIV-1 $_{\text{NL4-3-IN140/148}}$ replication competent virus [13] was pseudotyped with VSV-G to allow its entry in macrophages. Viral particles in the cell supernatant were harvested at 48 h post transfection, passed through 0.45 μm pore size filters and viral titers were determined by p24 content quantification by ELISA (PerkinElmer).

MDMs and PBLs (10^6) were infected with 100 ng p24 of HIV-1 $_{\text{AD8}}$, HIV-1 $_{\text{NL4-3}}$, HIV-1 $_{132\text{w}}$, HIV-1 $_{\text{BXO8}}$, HIV-1 $_{\text{DH12}}$, or the VSV-G envelope pseudotyped viruses (HIV-1 $_{\Delta\text{EnvNL4-3-Luc}}$, HIV-1 $_{\Delta\text{EnvNL4-3-IND64E}}$, or HIV-1 $_{\Delta\text{EnvNL4-3-IN140/148}}$) for 4 h at 37 °C. For HIV-1 long replication, MDMs or PBLs (10^6) were infected with 400 ng CAp24 of HIV-1 $_{\text{AD8}}$ or 200 ng CAp24 HIV-1 $_{\text{NL4-3}}$, respectively. Every 3 days, cell supernatants were harvested and replaced with fresh culture medium (10^6 MDMs/ml and 2×10^6 PBLs/ml) during 21 days. Viral replication was monitored by quantifying CAp24 release in the cell supernatants using the ELISA method (PerkinElmer). For viral cDNA detection with quantitative real-time PCR (qPCR), the viral stocks were pretreated with benzonase (Sigma) for 20 min at room temperature. The infections were determined by CAp24 content quantification by ELISA (Zeptometrix Crop) in the supernatant of cells, the luciferase activity from HIV-1 $_{\Delta\text{EnvNL4-3-Luc}}$ (VSV-G) in lysed cells using the Luciferase kit (Promega) and also by qPCR analysis of HIV-1 cDNA species at different time points. For HIV-1 $_{\text{CMV-GFP-I-SCEI}}$ (VSV-G) infection, HEK293T cells lines (0.5×10^5) were transfected with siSUGT1 or siCo siRNAs at 10 pmol in 500 μl complete medium using RNAi max (Qiagen). At 72 h post silencing, 1 μg of pCBASce plasmid encoding ISCEI endonuclease were transfected using Fugene (Promega). Six hours post-transfection, cells (0.2×10^6) were infected using 600 ng CAp24 of the virus for 2 h at 37 °C and then fresh medium was replaced and cells were cultured for further 48 h, detached and let to adhere on poly-L-lysine solution (Sigma) pretreated chamber slides for 2 h before fixation in 2% neutral buffered formalin (Sigma) for 10 min. For HIV-1 $_{\Delta\text{EnvNL4-3-GFP-Vpr}}$ (VSV-G) and HIV-1 $_{\text{IN-EGFP}}$ (VSV-G) infections, U2OS or HeLa cells (0.2×10^5) were seeded (in a well of eight wells chamber slides (BD)) and transfected at 10 pmol with siSUGT1 or siCo. siRNAs using RNAi max (Promega). Cells were then infected with 200 ng CAp24 of HIV-1 $_{\Delta\text{EnvNL4-3-GFP-Vpr}}$ (VSV-G) at 48 h post silencing for 4 h before 2% neutral buffered formalin (Sigma) fixation for 10 min. For HIV-1 $_{\text{IN-EGFP}}$ (VSV-G) infections, U2OS or HeLa cells at 48 h post-siRNA silencing were infected with

500 ng CAp24 of the virus with the addition of polybrene (10 µg/ml) during the different times of infection before fixation with 2% neutral buffered formalin (Sigma) or with cold methanol for EB1 staining. When U2OS cells were analyzed by live imaging microscopy, they were plated in ibidi 8-well chamber slides (ibiTreat) before siRNA transfection.

For the lentiviral vectors pLKO.1, pLKO.1-shSUGT1-3'UTR-1 (5'CCGGGCTCTCATCGTATTGTGTATACTC GAGTATACACAATACGATGAGAGC TTTTT3') and pLKO.1-shSUGT1-3'UTR-2: (5'CCGGATTGTGTATAT TCACCTAATGCT CGAGCATTAGGTGAATATACAC AATTTTTTG3'), pRLL-EF1-PGK-GFP, pRLL-EF1-SUGT1-PGK-GFP were produced by transfecting 3×10^6 HEK293T cells with 1 µg pDM2-VSV-G, 2.5 µg pΔ8.91 packaging and 2 µg the lentiviral vector using JetPRIME transfectant (Polyplus). Supernatants were harvested at 72 h post transfection and quantified for CAp24 content by ELISA. MDM (1×10^5) were transduced simultaneously using 1.5 µg CAp24 of each pLKO.1-shSUGT1 and/or 2 µg pRLL-EF1-SUGT1-PGK-GFP (pSUGT1) and/or with the equal amounts of control empty lentiviral vectors, with the addition of polybrene during transduction (10 µg/ml), for 6 h at 37 °C and then kept for 72 h before analysis by WB or infections. HEK293T cells (10^6) were infected with 20 ng CAp24 HIV-1_{ΔEnvNL4-3-Luc} (VSV-G) after 48 h of transfection with pCMV-SPORT6-SUGT1 (for SUGT1 bulk transfection) or pEGFP-N1-GFP control plasmid (for SUGT1 bulk transfection) or after 72 h of pRLL-EF1-SUGT1-PGK-GFP transfection and 24 h after GFP-based flow cytometry sorting.

Quantitative PCR

The quantification of the HIV-1 early reverse transcripts (ERT), late reverse transcripts (LRTs), 2-LTRs circles, and integrated proviruses were performed as previously described [10, 14]. DNA was extracted with the DNeasy Tissue Kit (Qiagen) at 6- and 24 h post infection (h.p.i.) for ERT detection, 24 and 72 h.p.i. for LRT and 2-LTRs detections, at 48 and 72 h.p.i. for integrated proviruses, respectively, in PBLs and MDMs. The qPCR analysis was carried on an ABI prism 7000 Sequence Detection System. The amounts of HIV-1 cDNA copies were normalized to the endogenous reference gene albumin. Standard curve was generated by serial dilutions of a commercial human genomic DNA (Roche).

Immunofluorescence, confocal microscopy, structured illumination microscopy (SIM), and live imaging

Brain autopsies of frontal cortex from three uninfected individuals and nine HIV-1 infected persons were obtained

in accordance with the Italian and EU legislations, after approval by the Institutional Review Board of the National Institute for Infectious diseases Lazzaro Spallanzani. Autopsies were deparaffinized, rehydrated, and subjected to high-temperature antigen retrieval (96 °C for 30 min) in 10 mM sodium citrate buffer, pH 6. After 1 h blocking in 0.1% bovine serum albumin (BSA) in PBS, autopsies were incubated at 4 °C for overnight with the primary antibodies anti-SUGT1 (Abcam, #ab30931) and anti-CAp24 (Abcam, #ab9044) diluted at 1/20 in 0.1% BSA in PBS. After three washings in PBS, the secondary antibodies anti-rabbit and anti-mouse IgG conjugated to Alexa-Fluor 488 (#A11001, #A11034) and 647 fluorochromes (#A21245) from Invitrogen, respectively, and/or the recombinant anti-ionized calcium-binding adaptor protein 1 (Iba1) conjugated to Alexa-Fluor 568 with Hoechst 33342 (Invitrogen, #1874027) for nuclei were added at 1/500 dilution for 2 h at room temperature. Immunostained autopsies were then mounted onto glass slides with Fluoromount G (Southern Biotech). At least five mosaic autopsy fields (115.33×115.33 µm each) were acquired by confocal microscopy (SP8, Leica) using a 63× objective. SP8 confocal microscope is equipped with two PMT and two high sensitivity hybrid detectors. Z series optical sections for autopsies were at 0.8 µm steps. HEK293T, HeLa, and U2OS cells were rinsed with PBS, fixed with 2% neutral buffered formalin (Sigma) for 10 min, permeabilized for 15 min with 0.3% Triton-X100 in PBS, washed twice in PBS and then blocked for 1 h at room temperature in 10% FBS in PBS prior to the incubation with the primary antibodies in 10% FBS in PBS for 2 h at room temperature. For anti-EB1 staining, the fixation was performed with cold methanol on ice for 2 min. After three washes in PBS, the secondary antibodies conjugated with Alexa-Fluor 488 (#A11001; #A11034), 546 (#A20189; #A11035), or 647 (#A21245) (1/500, Invitrogen) supplemented with Hoechst 33342 (Invitrogen, #1874027) for nuclei staining in 10% FBS in PBS were added to the cells for 30 min at room temperature. After three PBS washings, cells were then mounted with Fluoromount G (Southern Biotech), except for SIM visualization U2OS cells were mounted with ProLong antifade mountant (ThermoFisher Scientific) and incubated for 5 h at 30 °C prior analysis. The antibodies used for cells immunostaining were: anti-SUGT1 (BD Transduction Laboratories, #61204) for HEK293T cells and PBLs, anti-SUGT1 (Abcam, #ab30931) for U2OS cells, anti-HA (Biolegend, #90513), anti-phospho-H2AX (Ser139) (Millipore, #05-636), anti-α-tubulin (Sigma, #T9026), anti-α-tubulin (Curie Institute, A-R-H#02 2017), anti-acetylated α-tubulin on lysine 40 (Sigma, #T6793), anti-EB1 (BD transduction laboratories, #610535), anti-HIV-1-CAp24 (Abcam, #ab9044), and anti-Iba1-Alexa-Fluor 568 (Abcam, #ab221003). Cells were mainly imaged by confocal microscopy (SP8, Leica) using

hybrid detectors (pinhole airy: 0.6; pixel size: 180 nm) at optimal optical sectioning (OOS) of 0.2 μm . For acetylated α -tubulin and EB1 comets, the OOS was 0.11 μm . Fluorescence intensity related to SUGT1 and microtubule expressions was quantified by Image J software in the best focal plan for the total cell expression for at least 100 cells. The number of acetylated α -tubulin signals and the length of EB1 comets at the cell cortex were analyzed on maximum intensity of z projection images obtained by Image J software. Briefly, scan lines were drawn at the levels of cell cortex. Then, the number of fluorescence intensity peaks for acetylated α -tubulin and the length of EB1 comets were quantified using Image J software. The viral particles of HIV-1 $_{\Delta\text{EnvNL4-3-GFP-Vpr}}$ (VSV-G) immunofluorescence were performed as previously described [15] and then were visualized by confocal microscopy (SP8, Leica) using hybrid detectors (pinhole airy: 0.6; pixel size: 180 nm) and parameters adjusted for deconvolution by Huygens software (Scientific Volume). For U2OS cells, acquisitions were performed in 3D SIM mode, with a N-SIM structured illumination Nikon microscope before image reconstruction using the NIS Elements software. The system is equipped with an APO TIRF 100 \times 1.49NA oil immersion, a laser illumination (488 nm, 200 mW and 561 nm, 100 mW), and an EMCCD DU-897 Andor camera. Images were acquired with the following protocol: a Z stack (0.12 μm step) was acquired. Images were then reconstructed using Nikon elements software. The lateral resolution of SIM microscopy is about 32 nm. The distances between two different fluorochrome-labeled proteins for SIM microscopy images were calculated on one Z stack and using “Spot function> colocalize spot” functions of Imaris 5.7 software (Bitplane AG) on the cropped subcellular area where GFP-labeled HIV-1 particles were detected or not (HIV-1 GFP⁺ or HIV-1-GFP⁻). Briefly, this function determines the mass center of each fluorescent molecule on the raw SIM images and determines the event number of two colocalized molecules in predefined distance segment. Fluorescence from at least 300 molecules were quantified and the frequency of the events was determined by dividing the events number in each distance segment by the total event numbers of the analyzed area in the cytoplasm. For U2OS cells, images were also acquired with a high precision wide-field Eclipse NiU Upright Microscope (Nikon) equipped for image deconvolution. Acquisition was performed using a 100 \times Plan Apo VC 1.4 oil objective and a highly sensitive cooled interlined charge-coupled device camera (Roper CoolSnap HQ2). Acquired images were denoised using NdSafir software before deconvolution. All microscopy images with saturated signals were excluded. The colocalization threshold Mander’s correlation coefficient and the fluorescence spectrum overlap for colocalization were determined for different fluorochrome-labeled proteins using Image J

software, in the cropped subcellular area where GFP-Vpr-labeled HIV-1 was detected in the merged SIM images. The colocalization threshold Mander’s correlation coefficient (with values varying from 0 to 1) is used to quantify the colocalization or the co-occurrence proportion of two fluorescent probes in the same pixels of the region of interest or structure [16]. The threshold M1 was used to quantify the occurrence of green channel signals (HIV-1 $_{\text{IN-EGFP}}$) in the pixels of the detected red channel signals (α -tubulin). For live imaging, U2OS cells depleted for SUGT1 (siSUGT1) and control cells (siCo.) (0.5×10^5) plated in ibidi 8-well chamber slides (ibiTreat) were infected with HIV-1 $_{\text{IN-EGFP}}$ (VSV-G) (250 ng CAp24) in the presence of polybrene (10 $\mu\text{g/ml}$) and Hoechst 33342 (1 $\mu\text{g/ml}$) (Invitrogen) and imaged simultaneously at 1 h.p.i. using a confocal spinning disk (CSU-X1M1; Yokogawa) microscope (DMI6000; Leica) equipped with a CoolSnap HQ2 camera (Photometrics) in heating chamber at 37 $^{\circ}\text{C}$ with 5% CO_2 for further 3 h. Three field positions of each condition (siCo or siSUGT1) were imaged using a 63 \times oil lens (1.4 NA) every 20 min and with at least 40 series of Z stacks. The best focal plan images of the nucleus were then analyzed with Icy software for the mounting of the video and for quantification of infected cells with HIV-1 $_{\text{IN-EGFP}}$ RTCs/PICs in the nucleus or those with only cytoplasmic viral events.

Western blots and immunoprecipitations

Cells were lysed in NEHN lysis buffer (20 mM Hepes pH 7.5, 300 mM NaCl, 0.5% NP40, 20% glycerol, 1 mM EDTA) provided with protease and phosphatase cocktails inhibitors (Roche). Protein were quantified with the Protein assay kit (Biorad) and 30–50 μg of cell extracts were diluted in the Laemmli buffer (Biorad), boiled for 5 min at 95 $^{\circ}\text{C}$. Proteins were then loaded on the Nupage 10 or 12% Bis Tris gel (Life Technologies) for electrophoresis separation and blotted on the PVDF (0.45 μm) transfer membrane (Thermo Scientific). After blocking with 5% BSA, membranes were incubated with the primary antibodies followed by the secondary horseradish peroxidase (HRP) anti-rat and anti-rabbit, anti-mouse antibodies (Southern Biotech, #6180-01; #4050-05, and #1031-05, respectively). For co-immunoprecipitation assays, the Trueblot HRP secondary antibodies used were from eBioscience (#18-8816-33; #18-8817-33). The proteins were revealed by G:Box I CHEMI developer (Syngene, Ozyme) by using Super Signal West pico (Pierce) or ECL prime (GE healthcare). The primary antibodies used were: anti-SUGT1 (BD Transduction Laboratories, #61204), anti-HA (3F10, Roche, #11867423001), anti-GAPDH (Millipore; #MAB374), anti-CAp24 (NIH AIDS research reagents, #4250), anti-Actin (Abcam, #ab49900), anti-acetylated α -tubulin K40 (AcK40-

α -tubulin) (Sigma, #T6793), anti- α -tubulin (Sigma, #T9026), and anti-HIV-1 integrase (IN-2) (Santa-Cruz, #sc-69721) in 5% skimmed milk in TBS-1% tween. For immunoprecipitations, HEK293T cells expressing HA-IN through transfection at 48 h post transfection or U2OS cells infected for 4 h with HIV-1 $_{\Delta\text{EnvNL4-3-Luc}}$ (VSV-G) were harvested and then lysed in NEHN buffer. Anti-HA (3F10; Roche, #11867423001) or anti-SUGT1 (Abcam, #ab30931) (2.5 μg) were added to the cell lysates (1 mg) for 12 h incubation at 4 °C on the wheel. Then, 30 μl of the protein G sepharose four fast flow beads (GE healthcare) were added for additional 4 h incubation. Immunocomplexes immobilized on the beads were washed twice with NEHN buffer (300 mM NaCl) and third time with NEHN buffer (500 mM NaCl), resuspended in Laemmli buffer (Biorad) and boiled at 95 °C for 5 min. Immunocomplexes were then analyzed by WB.

Statistical analysis

We used the two-tailed unpaired *t*-test for two group comparison and the two-way ANOVA test for the multiple comparisons (more than two groups) of the absolute values means, means of frequencies, or means of fold changes \pm SEM (standard error of the mean). Fold changes were calculated as the ratio of the mean value from the treated sample to the mean value of the control sample. The statistical tests were represented in the figures for $n > 10$ sample size. When $n < 10$, the experiments were represented as individual data points without error bars. Data were analyzed with Graphpad prism 6 software. Statistical significance was given as * $p < 0.05$, ** $p < 0.01$, *** $p < 0.001$, and **** $p < 0.0001$.

Results

The SUGT1 protein promotes permissiveness to HIV-1 infection

Confocal immunofluorescence microscopy was used to evaluate SUGT1 expression at the single cell level in brain frontal cortex sections from HIV-1 infected and uninfected persons. Interestingly, infected cells expressed higher levels of SUGT1, as compared with uninfected cells within the same HIV-1 patient brain section or cells in the brain sections of uninfected controls (Fig. 1a–d). These cells also expressed the Iba1 (Supplementary Fig. S1a), indicating that SUGT1 is increased in macrophages/microglia of HIV-1 patient brain sections. Furthermore, SUGT1 expression was increased in activated T cells, which are susceptible to HIV-1 infection as compared with resting primary T lymphocytes, which resist HIV-1 infection (Fig. 1e and

Supplementary Fig. S1b). The expression of SUGT1 also strongly increased in primary MDMs, which are permissive for HIV-1, compared with monocytes, which are refractory to HIV-1 infection (Fig. 1f and Supplementary Fig. S1c), indicating that SUGT1 expression increases in permissive cells. We then analyzed the impact of SUGT1 depletion on HIV-1 replication. SUGT1 was silenced using a smart pool of siRNAs (siSUGT1) in MDMs (Fig. 1g). SUGT1-depleted MDMs were infected with R5-tropic HIV-1 $_{\text{AD8}}$, and viral replication was determined by quantifying CAP24 release. SUGT1 depletion strongly suppressed HIV-1 replication without affecting cell viability (Fig. 1j, k and Supplementary Fig. S1d). These results were confirmed in activated PBLs (Fig. 1h, m and Supplementary Fig. S1e, f) and in cervical epithelial (HeLa) cells engineered to express CD4/CXCR4 and a Tat-inducible β -galactosidase (Fig. 1i, n and Supplementary Fig. S1g). These results were corroborated using a different SUGT1 siRNA (siSUGT1-1) (Supplementary Fig. S1h–j) and revealed no effects on CD4 and CXCR4 expression levels nor on cell viability (Supplementary Fig. S1k, l). In addition, long-term analysis of CAP24 release from MDMs or PBLs that were infected, respectively, with R5-tropic HIV-1 $_{\text{AD8}}$ or X4-tropic HIV-1 $_{\text{NL4-3}}$ (Fig. 1o, p and Supplementary Fig. S1m–p) showed that SUGT1 depletion abolished HIV-1 replication and further indicated that SUGT1 is a permissive factor for HIV-1 infection.

The early pre-integrative steps of HIV-1 life cycle are controlled by SUGT1

To identify the viral replication steps that are controlled by SUGT1, MDMs, and PBLs were silenced for SUGT1 and infected with *luciferase* (Luc)-expressing HIV-1 $_{\Delta\text{EnvNL4-3-Luc}}$ (HIV-1 $_{\text{VSV-G}}$), which is defective in the HIV-1 envelope and pseudotyped with a VSV-G envelope (which allows the virus to enter cells by endocytosis). SUGT1 depletion strongly reduced the infectivity of HIV-1 $_{\Delta\text{EnvNL4-3-Luc}}$ (VSV-G) in MDMs (Fig. 2a, b) and PBLs (Fig. 2c, d), implying that SUGT1 modulates post-entry steps. In MDMs (Fig. 2e) and PBLs (Fig. 2f) whose SUGT1 had been depleted by a pool of two short hairpin RNAs (shSUGT1), the expression of SUGT1 cDNA resistant to shSUGT1 restored the infectivity of HIV-1 $_{\Delta\text{EnvNL4-3-Luc}}$ (VSV-G) (Fig. 2g (for MDMs) and Fig. 2h (for PBLs)). Consistently, the exogenous SUGT1 overexpression in HEK293T cells significantly enhanced the infectivity of HEK293T cells with HIV-1 $_{\Delta\text{EnvNL4-3-Luc}}$ (VSV-G) (Supplementary Fig. S2a–d), demonstrating the specific effect of SUGT1 in promoting HIV-1 infection.

MDMs and PBLs were then depleted for SUGT1, infected with the same virus, and analyzed by qPCR for ERT (at 24 and 6 h.p.i. of MDMs and PBLs, respectively),

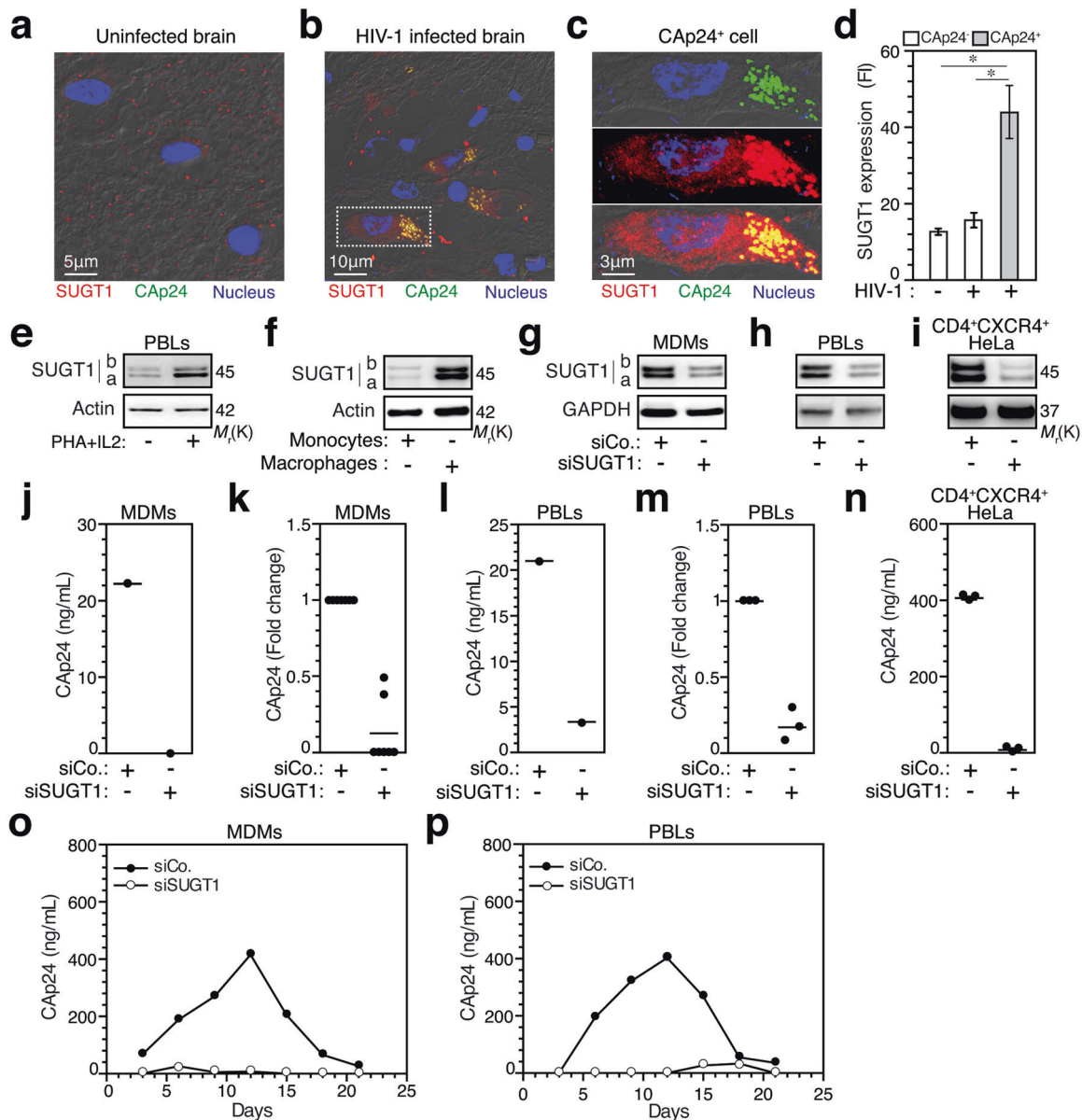


Fig. 1 SUGT1 determines HIV-1 permissiveness in human cells. **a–c** Immunofluorescence of brain autopsies from uninfected persons ($n = 3$) and HIV-1 infected patients ($n = 3$) for SUGT1, CAp24, and nucleus. **c** Magnification. **d** Quantification of SUGT1 expression in CAp24⁺ ($n = 45$) or CAp24⁻ ($n = 690$) cells detected in brain sections. Fluorescence intensities (FI) are shown. Means \pm SEM are indicated. P values were calculated using two-tailed unpaired t -test using Bonferroni correction ($*p < 0.1$). Representative human resting/PHA-P/IL2-activated PBLs (**e**) or monocytes/macrophages (**f**) WB of endogenous SUGT1 levels are shown ($n = 3$). SUGT1 a and b

isoforms are indicated. SUGT1 depletion in human MDMs (**g**), PBLs (**h**), and CD4⁺CXCR4⁺ HeLa cells (**i**) are shown ($n = 3$). Effect of SUGT1 depletion on viral production obtained from MDMs (**j**, **k**), PBLs (**l**, **m**), or CD4⁺CXCR4⁺ HeLa cells ($n = 3$) (**n**) infected with HIV-1_{AD8} (**j**, **k**) or HIV-1_{NL4-3} (**l–n**). CAp24 release for representative donor (**j**, **l**) and fold changes ($n = 7$ for MDMs, $n = 3$ for PBLs) (**k**, **m**) are shown. Effect of SUGT1 depletion on viral production obtained at indicated times post infection from MDMs (**o**) and PBLs (**p**) infected with HIV-1_{AD8} (**o**) or HIV-1_{NL4-3} (**p**). CAp24 release from representative donors is shown ($n = 3$).

LRTs, and 2-LTR circles (at 72 and 24 h.p.i, respectively), as well as integrated proviruses (at 72 and 48 h.p.i, respectively). No significant difference in the formation of HIV-1 ERT was observed in SUGT1-depleted cells (Fig. 2i, j). A mild decrease of the LRTs was observed in SUGT1-depleted MDMs (Fig. 2k) or PBLs (Fig. 2l) (as compared with control cells). More importantly, SUGT1 depletion

strongly inhibited the formation of 2-LTR circles, a surrogate marker of nuclear viral import, in HIV-1-infected MDMs (Fig. 2m) and PBLs (Fig. 2n). Consequently, the integrated proviruses (detected by the Alu-nested qPCR) were decreased after SUGT1 depletion (Fig. 2o, p). Similar results were obtained when SUGT1-depleted MDMs were infected with R5-tropic HIV-1_{AD8} (Supplementary

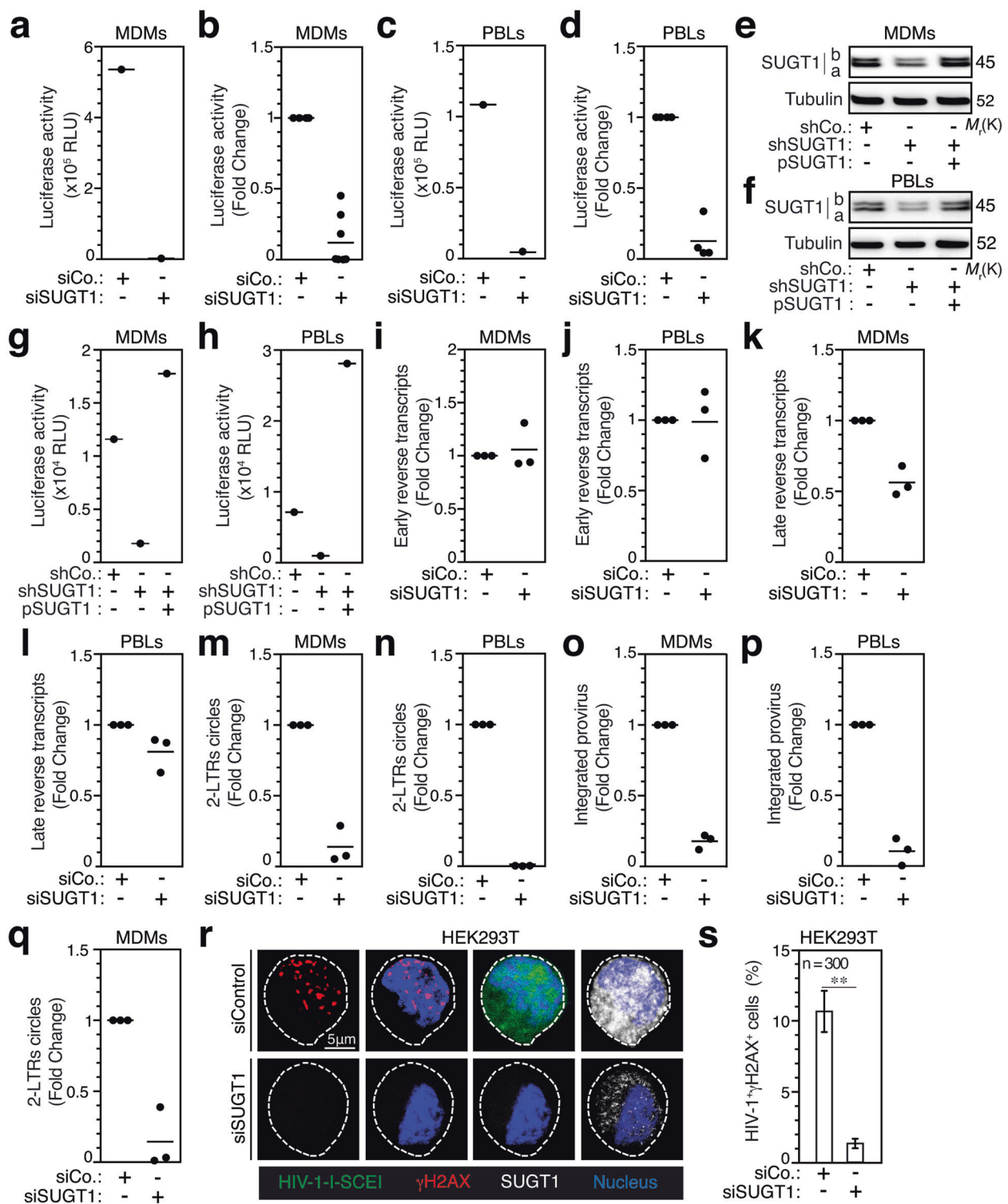


Fig. S2e–h). The nuclear import (as evaluated by 2-LTR circles qPCR) of a HIV-1 mutant that is defective for integration (HIV-1 Δ EnvNL4-3-IND64E (VSV-G)) was also abrogated by the depletion of SUGT1 (Fig. 2q). Considering that mutant HIV-1 Δ IND64E translocates efficiently to the nucleus [17], this result implies that SUGT1 regulates HIV-

1 pre-integrative phases. To further characterize this process, we infected SUGT1-depleted HEK293T cells with HIV-1 Δ CMVGFP-I-SCEI (VSV-G), which encodes GFP as reporter gene and has been engineered by inserting, into the viral DNA, the yeast ISCEI endonuclease cleavage site that is cut when its cognate enzyme is introduced into human

◀ **Fig. 2 SUGT1 promotes early HIV-1 replication steps.** **a–d** HIV-1 infectivity of control or SUGT1-depleted MDMs (**a, b**) and activated PBLs (**c, d**) that were infected with HIV-1 $_{\Delta\text{EnvNL4-3-Luc}}$ (VSV-G) for 72 h. Luciferase activity from representative donor (**a, c**) and fold changes ($n = 8$ for MDMs and $n = 4$ for PBLs) (**b, d**) are shown. **e–h** MDMs and PBLs were transduced with lentiviral vectors expressing control (shCo.), a pool of two shRNAs against SUGT1 (shSUGT1), and/or SUGT1 resistant cDNA (pSUGT1) for 72 h prior infection with HIV-1 $_{\Delta\text{EnvNL4-3-Luc}}$ (VSV-G). WB (**e, f**) and luciferase activity at 48 h.p.i. from representative donors are shown (**g, h**) ($n = 3$). Fold changes of HIV-1 early reverse transcripts (**i, j**), late reverse transcripts (**k, l**), 2-LTRs circles (**m, n, q**), and integrated proviruses (**o, p**) were determined by qPCR in control or SUGT1-depleted macrophages (**i, k, m, o, q**) or lymphocytes (**j, l, n, p**) that were infected with HIV-1 $_{\Delta\text{EnvNL4-3-Luc}}$ (VSV-G) (**i–p**) or with HIV-1 $_{\Delta\text{EnvNL4-3-IND64E}}$ (VSV-G) (**q**) ($n = 3$). Representative confocal micrographs of HIV-1 $_{\text{CMV-GFP-I-SCEI}}$ -infected HEK293T cells (**r**) and percentages of HIV-1 infected (GFP $^{+}$) cells with γH2AX^{+} foci (**s**) are shown. Means \pm SEM are indicated ($n = 3$). *P* values were calculated using two-tailed unpaired *t*-test (** $p < 0.01$).

cells [11]. In this system, the depletion of SUGT1 in HEK293T cells strongly inhibited HIV-1 infection, as revealed by the reduction of the percentage of cells that express immunofluorescent γH2AX -associated foci as well as the expression of virus-encoded GFP (Fig. 2r, s). The lack of GFP detection in SUGT1-depleted cells indicates the absence of 2-LTR's circles forms (which can express the GFP reporter gene) and further suggests that SUGT1 governs the nuclear translocation of HIV-1. Altogether, these data imply that SUGT1 expression dictates HIV-1 permissiveness by promoting HIV-1 reverse transcription and mainly nuclear import.

SUGT1 is associated with microtubules bearing HIV-1

Considering the role of SUGT1 in the stabilization and attachment of proteins to the microtubule network [4], we investigated the presence of SUGT1 on microtubules bearing HIV-1. U2OS cells were infected with a VSV-G-pseudotyped HIV-1 $_{\Delta\text{EnvNL4-3}}$, which incorporates GFP-Vpr (HIV-1 $_{\Delta\text{EnvNL4-3-GFP-Vpr}}$ (VSV-G)) [15], and the subcellular localization of SUGT1, GFP-labeled viral complexes, and microtubules were analyzed by super-resolution SIM and wide-field high precision microscopy at 4 h post infection. As expected, at this time point, GFP-labeled viral complexes colocalized with cytoplasmic filaments (Fig. 3aI) and aggregated at microtubule-organizing centers (MTOC) (Supplementary Fig. S3a). Importantly, endogenous SUGT1 molecules were located in close proximity to the microtubule-associated viral complexes (Fig. 3aII). SUGT1, viral complexes, and microtubules often formed ternary structures (Fig. 3aIII–4). Fluorescence overlap spectrum analysis confirmed these results, indicating that the three components (SUGT1, GFP, and microtubules) were located within a distance of $<0.8 \mu\text{m}$ (Fig. 3aIII–4). A

high colocalization Mander's coefficient (~ 1) confirmed the tight association of SUGT1 with microtubules that are used by HIV-1 for trafficking in host cells (Supplementary Fig. S3b, c).

Since HIV-1 integrase (IN) translocates to the nucleus to catalyze the integration of viral cDNA into the human genome, we monitored the subcellular localization of HA-IN in SUGT1-depleted U2OS cells. Interestingly, we observed that the silencing of SUGT1 (Fig. 3b) induced a diffused localization of IN in the cytoplasm and the nucleus compared with control cells that had exclusive nuclear localization (Fig. 3c, d), indicating that SUGT1 contributes to the nuclear accumulation of IN. In agreement with a previous report showing that efficient nuclear translocation prevents cytoplasmic degradation of HIV-1 IN [18], protein levels of HA-IN decreased in SUGT1-depleted cells (Fig. 3b). However, no interactions between endogenous SUGT1 and HA-IN were detected by co-immunoprecipitation in HEK293T cells (Fig. 3e), suggesting that SUGT1 may act on HIV-1 nuclear translocation without interacting with viral proteins. Altogether, these data indicate that SUGT1 is associated with microtubules bearing HIV-1.

SUGT1 regulates the organization and the stability of the cortical microtubule plus-ends

To understand the mechanism by which SUGT1 contributes to HIV-1 nuclear import, we investigated the effect of SUGT1 on the structural organization of microtubules. Although SUGT1 knockdown did not modify tubulin expression, nor disrupt the global architecture or the density of the microtubule network (Fig. 4a, b and Supplementary Fig. S4a, b), confocal microscopy revealed a significant alteration of the microtubule plus-ends (+MTs) organization at the level of the cell cortex (Fig. 4a, c and Supplementary Fig. S4a). SUGT1-depleted U2OS cells exhibited +MTs that were dissociated and distributed perpendicularly to the cell cortex, while in control cells, the +MTs were clustered and curved in parallel to the cell cortex. Even though the total expression of stable microtubules (AcK40 α -tubulin) was not affected by the SUGT1 knockdown (Supplementary Fig. S4b), the acetylation of +MTs at the cell cortex significantly decreased in U2OS and HeLa cells (Fig. 4d–f and Supplementary Fig. S4c–f). These data indicate that the cortical +MTs, which are the first contact points of HIV-1 with the microtubule network after viral entry, are unstable in SUGT1-depleted cells and thus may not efficiently support the cytoplasmic trafficking of the virus. To confirm this hypothesis, we analyzed whether SUGT1 depletion would affect the organization of the plus-end tracking protein EB1, which promotes the cytoplasmic trafficking of HIV-1 on microtubules [1]. Considering that EB1 molecules bind to +MTs and form EB1 comets, whose

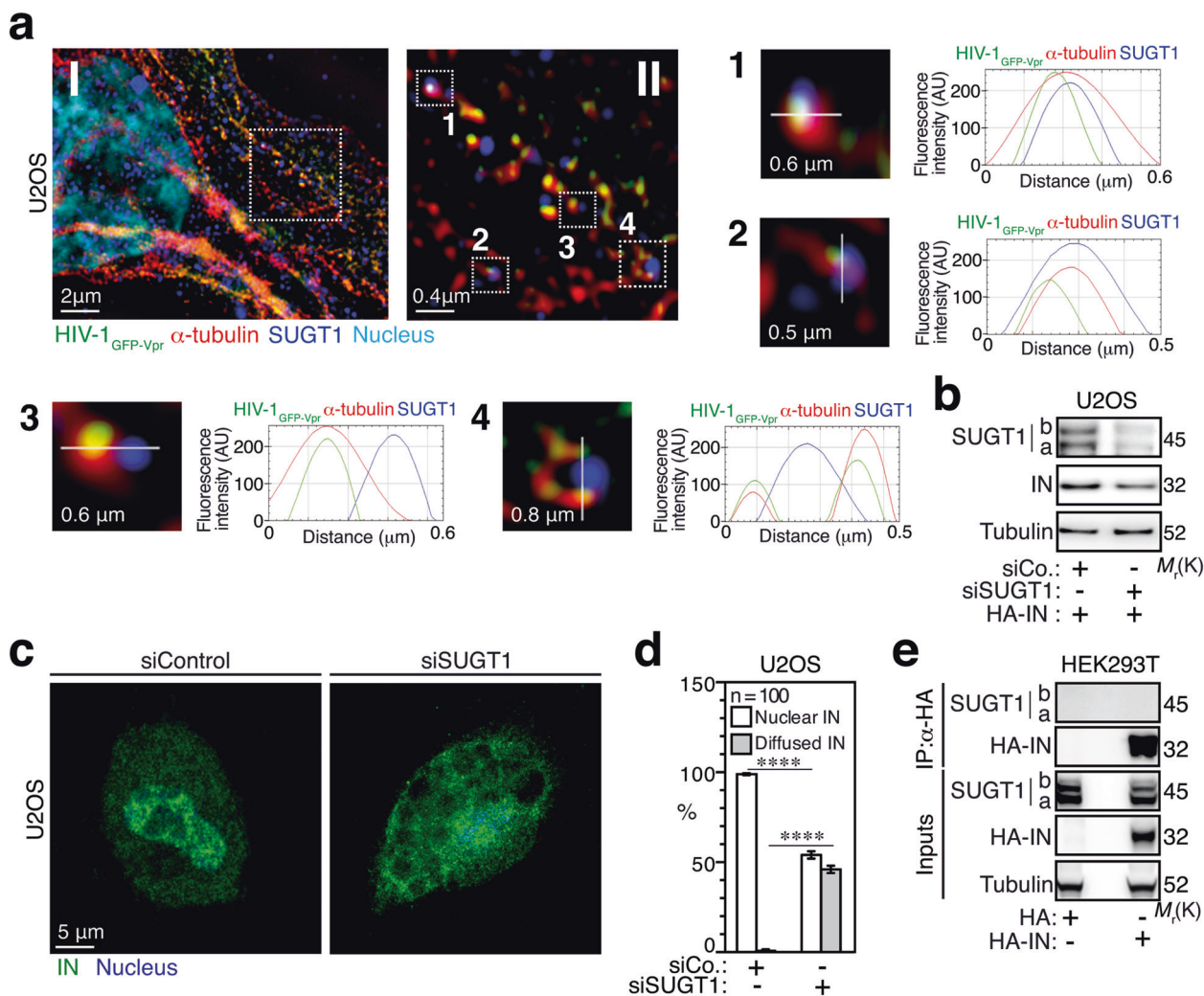


Fig. 3 SUGT1 is associated with microtubules trafficking HIV-1. **a** Representative SIM micrograph of 4 h HIV-1 $_{\Delta\text{EnvNL4-3-GFP-Vpr}}$ (VSV-G)-infected U2OS cells showing SUGT1 and α -tubulin expression (**aI**). **aII** is a magnification of the dashed region in **aI**. **aIII–4** are the magnifications of the dashed regions in **aII**. Fluorescence overlap spectrums of **aIII–4** cropped regions, are shown. **b** HIV-1 IN and SUGT1 expression levels by WB in control and SUGT1-depleted U2OS cells after 48 h siRNA transfection and expression of exogenous HIV-1 IN for 24 h. Representative confocal micrographs of HIV-1

HA-IN expression in control and SUGT1-depleted U2OS cells (**c**) and percentages of cells showing nuclear or diffused HIV-1 IN (**d**). **e** Immunoprecipitation of HA-IN in control and HA-IN-overexpressing HEK293T cells and expression of indicated proteins by WB. WB and images are representative of three independent experiments. Means \pm SEM are indicated from at least three independent experiments. *P* values were calculated using the two-way ANOVA test (*****p* < 0.0001).

elongation is associated with an increased growth rate and a decreased stability [19–22], the impact of SUGT1 silencing on the length of EB1 comets was determined. A significant increase in the length of EB1 comets was observed in SUGT1-depleted HeLa and U2OS cells, compared with control cells (Fig. 4g–i and Supplementary Fig. S4g–j), suggesting that in SUGT1-depleted cells, +MTs are less stable and highly dynamic, and thus would not sustain the trafficking of HIV-1 viral particles after viral entry. Taken together, our data reveal that SUGT1 controls the architecture and the stability of +MTs, which are required for the attachment and efficient trafficking of HIV-1 on the microtubule network.

SUGT1 is essential for the association of HIV-1 with stable microtubules and its translocation to the host cell nucleus

Co-immunoprecipitation assays revealed an interaction between SUGT1 and stable microtubules (Fig. 5a). This interaction was strongly enhanced after 4 h of infection of U2OS cells with HIV-1 $_{\Delta\text{EnvNL4-3-Luc}}$ (VSV-G), further demonstrating that SUGT1 is associated with the microtubules that are used by HIV-1 for trafficking (Fig. 5a). Using HIV-1_{IN-EGFP} virus pseudotyped by VSV-G envelope that contains enhanced GFP-labeled IN [12, 23], we showed that in SUGT1-depleted U2OS cells, and in

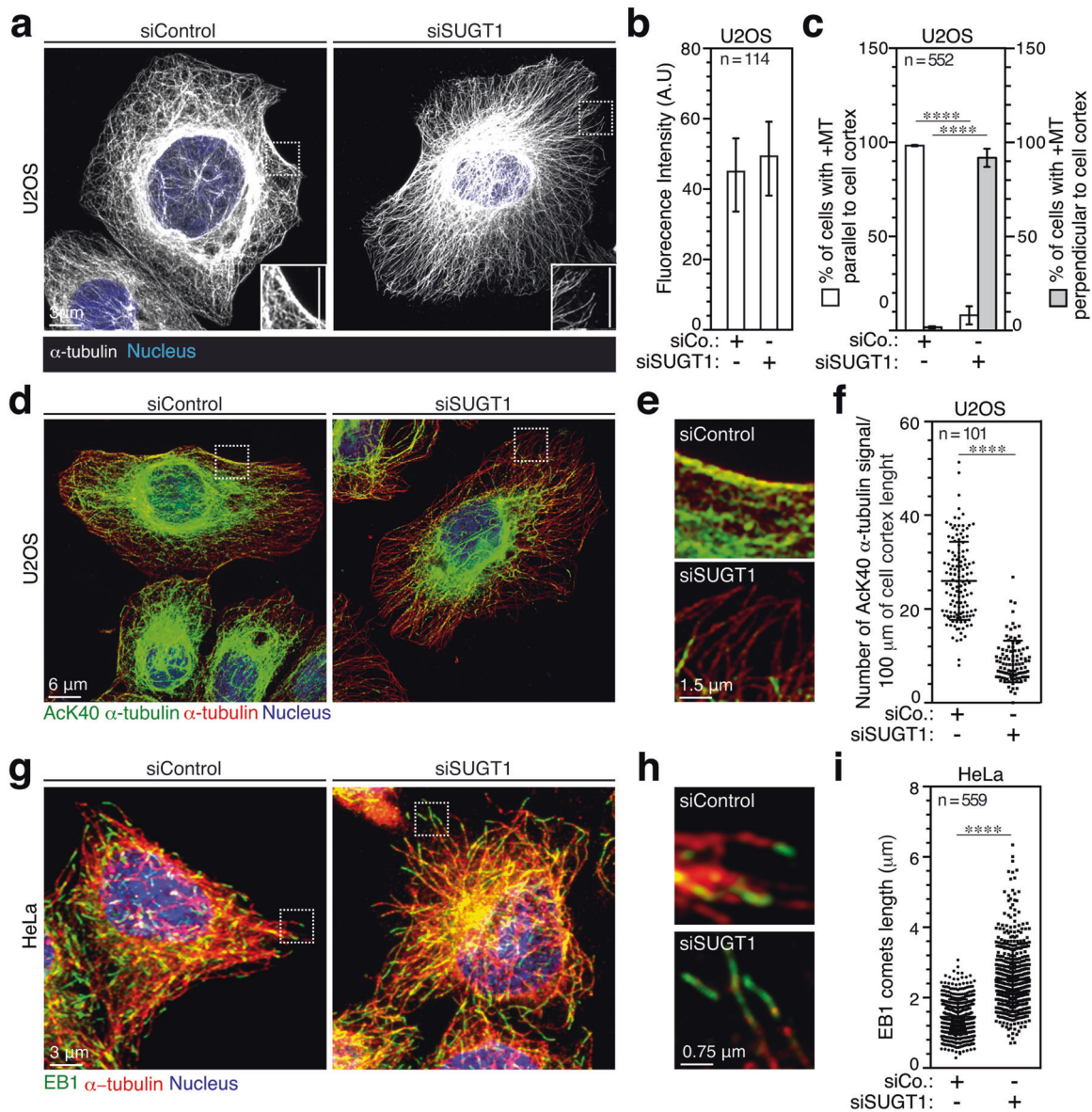


Fig. 4 SUGT1 stabilizes microtubule tips at the cell cortex. **a** Representative confocal micrographs and magnifications showing α -tubulin and nucleus in control and SUGT1-depleted U2OS cells. **b** Fluorescence intensity of α -tubulin. **c** Percentages of cells with +MTs parallel or perpendicular to the cell cortex. **d–f** Representative confocal micrographs of α -tubulin, AcK40 α -tubulin, and nucleus in control and SUGT1-depleted U2OS cells. Magnifications (**e**). Quantification of AcK40 α -tubulin signals normalized to 100 μ m of cell

cortex length in cells (**f**). (**g–i**) Representative confocal micrographs of α -tubulin, EB1, and nucleus in control and SUGT1-depleted HeLa cells. Separate fluorescence images of **g** are shown in Supplementary Fig. S4g, **h**. Magnifications (**h**). Quantification of EB1 comet length ($n = 559$) of cells ($n = 60$) (**i**). Means \pm SEM are indicated from at least three independent experiments. P values were calculated using the two-way ANOVA test for **c** and two-tailed unpaired t -test for **f** and **i** (**** $p < 0.0001$).

contrast to control cells (Fig. 5b), HIV-1_{IN-EGFP}⁺ viral complexes did not aggregate at the MTOC and displayed a diffuse distribution in the cytoplasm (Fig. 5d). Accordingly, the colocalization of HIV-1_{IN-EGFP}⁺ complexes with microtubules significantly decreased in SUGT1-depleted cells (Fig. 5c), suggesting that, in the absence of SUGT1, a defect in the migration to the perinuclear area is associated with a defect in the association of the virus with

microtubules. In agreement with the results obtained with HIV-1 IN expressed as a single protein (Fig. 3b), the mean fluorescence intensity of HIV-1_{IN-EGFP}⁺ complexes detected after 4 h of infection of SUGT1-depleted cells was significantly decreased, as compared with control cells (Supplementary Fig. S5a), indicating that the failed nuclear translocation of HIV-1 induces its rapid cytoplasmic degradation. Moreover, SUGT1 depletion

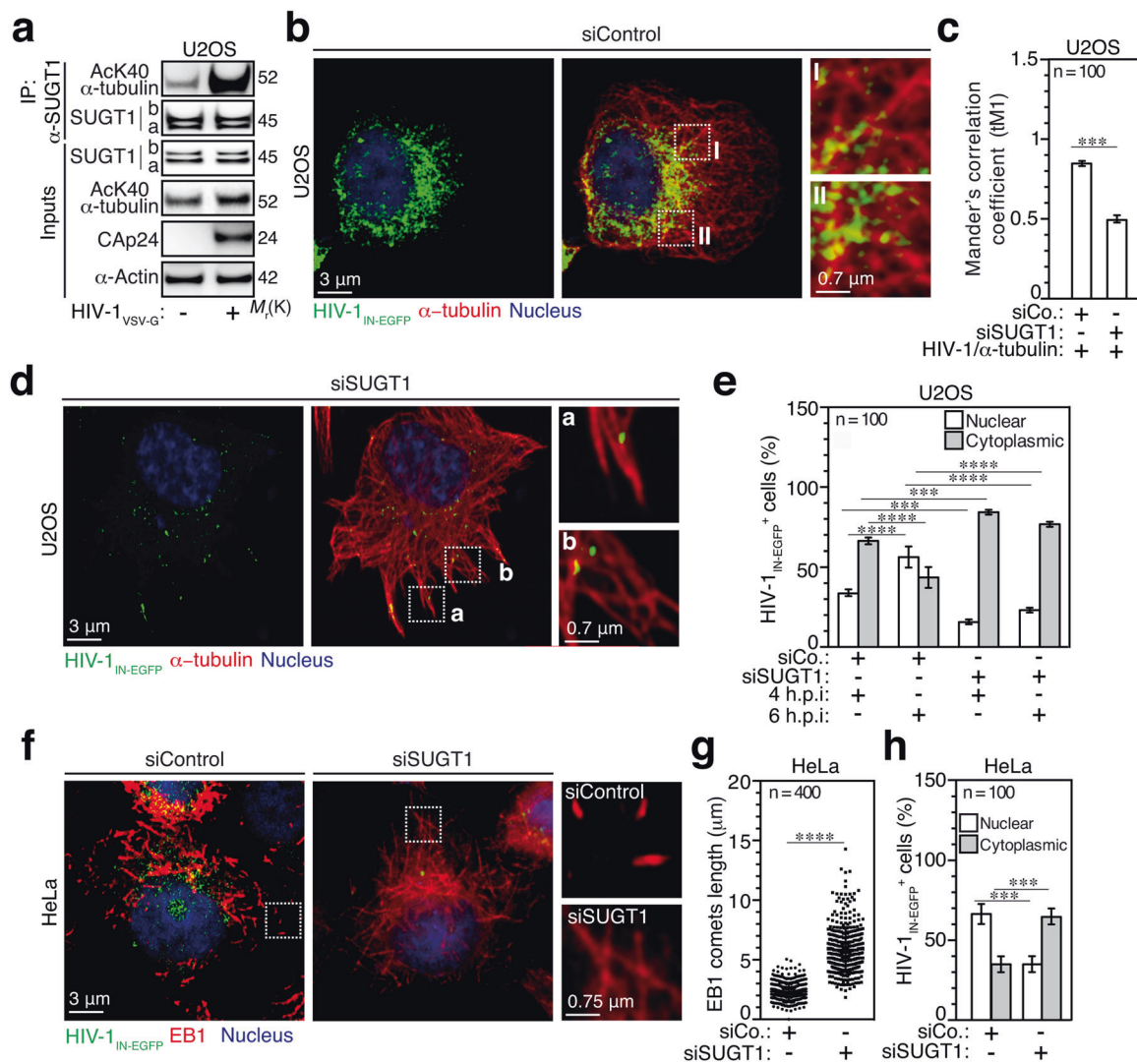


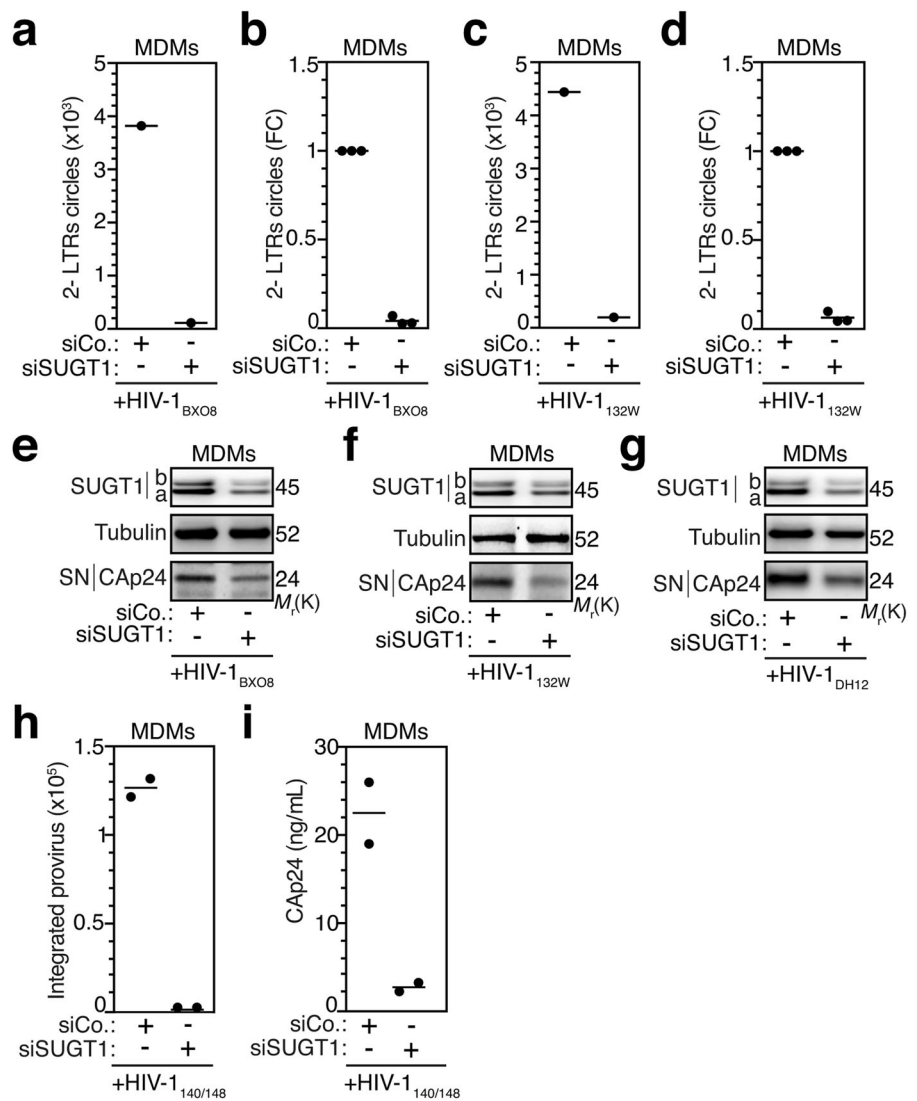
Fig. 5 SUGT1 promotes the association between HIV-1 and microtubules. **a** Co-immunoprecipitation of endogenous SUGT1 with AcK40 α -tubulin in control and HIV-1 $_{\Delta\text{EnvNL4-3-Luc}}$ (VSV-G)-infected U2OS cells for 4 h and expression of indicated proteins by WB. Representative confocal micrographs of HIV-1 $_{\text{IN-EGFP}}$ virus and α -tubulin in control (**b**) and SUGT1-depleted (**d**) U2OS cells that were infected for 4 h. **c** Mander's correlation coefficient (tM1) of HIV-1 $_{\text{IN-EGFP}}^+$ and α -tubulin in control and SUGT1-depleted U2OS cells at 4 h.p.i. **e** Percentages of cells showing nuclear or cytoplasmic HIV-1 $_{\text{IN-EGFP}}^+$ events at 4

and 6 h.p.i. **f** Representative confocal micrographs of HIV-1 $_{\text{IN-EGFP}}$, EB1 and nucleus in control and SUGT1-depleted HeLa cells that were infected with HIV-1 $_{\text{IN-EGFP}}$ for 6 h. Magnifications are shown. **g** Lengths of EB1 comets ($n = 400$) are determined. **h** Percentages of control or SUGT1-depleted HeLa cells showing nuclear or only cytoplasmic HIV-1 $_{\text{IN-EGFP}}^+$ events at 6 h.p.i. Means \pm SEM are indicated from at least three independent experiments. P values were calculated using two-tailed unpaired t -test for **c** and **g** and two-Way ANOVA for **e** and **h** (*** $p < 0.001$ and **** $p < 0.0001$).

decreased the percentage of cells with HIV-1 $_{\text{IN-EGFP}}$ nuclear events at 4 and 6 h.p.i. and increased the percentage of cells showing only cytoplasmic viral events (Fig. 5e). Consistent with these results, live imaging microscopy showed nuclear translocation of HIV-1 $_{\text{IN-EGFP}}^+$ viral complexes in control U2OS cells (Movie 1), while in the SUGT1-depleted cells, viral complexes did not translocate to the host cell nucleus (Movie 2), leading to a decrease of HIV-1 nuclear events (Supplementary Fig. S5b). Interestingly, a significant elongation of EB1

comets was detected in SUGT1-depleted HeLa cells infected with HIV-1 $_{\text{IN-EGFP}}$ (VSV-G) (Fig. 5f, g) or HIV-1 $_{\Delta\text{EnvNL4-3-Luc}}$ (VSV-G) (Supplementary Fig. S5c) for 6 h, as compared with control cells. Accordingly, the nuclear accumulation of HIV-1 $_{\text{IN-EGFP}}^+$ viral complexes was significantly decreased in SUGT1-depleted cells (Fig. 5h). Altogether, these results demonstrate that SUGT1 promotes HIV-1 nuclear import by increasing its association with microtubules and its cytoplasmic trafficking to reach the host nucleus.

Fig. 6 SUGT1 depletion impairs replication of HIV-1 primary isolates and ART resistant virus. HIV-1 2-LTRs circles quantification by qPCR 72 h.p.i. with HIV-1_{BX08} (**a, b**) and HIV-1_{132W} (**c, d**) primary isolates of control and MDMs that were silenced for SUGT1 during 72 h. Representative donor (**a, c**) and fold changes ($n = 3$) (**b, d**) are shown. HIV-1-CAP24 detected by WB in the cell supernatants (SN) of MDMs that were depleted (or not) for SUGT1 and infected with HIV-1_{BX08} (**e**), HIV-1_{132W} (**f**), and HIV-1_{DH12} (**g**). Representative WB revealing CAP24, SUGT1, and Tubulin expressions are shown ($n = 3$). **h, i** Control and SUGT1-depleted primary human MDMs were infected with HIV-1_{140/148} and evaluated for proviral integration and for CAP24 release at 72 h.p.i. ($n = 2$).



SUGT1 depletion abolished permissiveness to HIV-1 primary isolates and antiretroviral treatment (ART)-resistant viral mutant

In order to evaluate the potential of SUGT1 inactivation for HIV-1 therapy, we determined the impact of SUGT1 depletion on the permissiveness of MDMs to infection with HIV-1 primary isolates (HIV-1_{BX08}, HIV-1_{132W}, and HIV-1_{DH12}) and to HIV-1 clone (HIV-1_{140/148}), a double mutant virus that is resistant to raltegravir ART [13]. Interestingly, SUGT1 depletion strongly inhibited the formation of 2-LTR circles (Fig. 6a–d) and CAP24 release (Fig. 6e–g) from MDMs that were infected with CCR5 (R5) tropic (HIV-1_{BX08} and HIV-1_{132W}) or CCR5/CXCR4 (R5X4) dual tropic (HIV-1_{DH12}) HIV-1 primary isolates (Fig. 6a–e). In addition, the depletion of SUGT1 drastically impaired viral integration (Fig. 6h) and CAP24 release (Fig. 6i) from MDMs that were infected with an HIV-1 double mutant

G140S-Q148H in integrase polypeptide (HIV-1_{140/148}) that is resistant to the integrase inhibitor raltegravir. Altogether, these results highlight the potential for SUGT1 as a cellular target to inhibit viral replication and overcome viral resistance to ART.

Discussion

In the present study, we demonstrate that SUGT1 is a host factor that determines lymphocyte and macrophage susceptibility to HIV-1 infection and replication via an effect on the post-entry replication steps. SUGT1 stabilizes the +MTs, thereby promoting the association of HIV-1 with stable microtubules, allowing their efficient trafficking to the nuclear pores, and viral import into the nucleus and subsequent integration into the host genome. In contrast to the previously described microtubule-associated proteins

(such as EB1 and Kif4 [1–3, 24]), which increase microtubule stability (by enhancing AcK40 α -tubulin) following infection, SUGT1 contributes to maintain the stability of microtubules mainly at the level of the plus-end TIPs, by inhibiting their dynamic and preserving their acetylation. The fact that we showed that SUGT1 expression is upregulated in the HIV-1 permissive activated T cells and macrophages with respect to their cognate resting lymphocytes and monocytes refractory to HIV-1 infection, does not exclude the possible contribution of synergetic pathways involved during differentiation and activation in the stabilization of the microtubules and enhancing the susceptibility to HIV-1. A recent report demonstrated that the rapid proteasome-mediated degradation of the viral cores in the cytoplasm is detected when their uncoating fails to occur progressively up to their trafficking to the nuclear pores [25]. Consistent with this report, the intensity of the fluorescent viral complexes, which were mainly accumulated in the cytoplasm of host cells, was significantly decreased in SUGT1-depleted cells, as compared with control cells, suggesting their degradation by proteasomes due to lack of efficient trafficking to the nuclear pores. Similarly, HIV-1 IN was shown to be stabilized on the MTOC, prior to its nuclear translocation, through direct interaction with microtubule-associated proteins (such as the centrosomal protein STU2P (yeast homolog of XMAP215) and the dynein light chain protein DYN2P) [26, 27] and its failure to be recruited to the nucleus leads to its rapid degradation by proteasomes in the cytoplasm of host cells [18]. Future studies will explore the potential role of SUGT1 in the trafficking of other viruses that employ the microtubule network, such as Hepatitis C virus, Dengue virus, or African Swine Fever virus. Finally, our results demonstrate that SUGT1 should be considered as a target in novel therapeutic strategies to inhibit infection with HIV-1 strains that are resistant to raltegravir ART.

Acknowledgements We acknowledge Dr Alessandro Donado, Yann Lecluse, Floriane Herit, and Pierre Bourdoncle (IMAG'IC facility of Institut Cochin) for their technical support, and Pr. Eric Solary for the pRLL-EF1-PGK-GFP lentiviral vector plasmid. This work was supported by funds from Agence Nationale de la Recherche (ANR-10-IBHU-0001, ANR-10-LABX33, and ANR-11-IDEX-003-01), Canc eropole Ile de France, Electricit e de France, Fondation Gustave Roussy, Institut National du Cancer (INCA 9414), NATIXIS, SIDACTION, and the French National Agency for Research on AIDS and viral Hepatitis (ANRSH) (to J-LP and FN).

Compliance with ethical standards

Conflict of interest The authors declare that they have no conflict of interest.




Publisher's note Springer Nature remains neutral with regard to jurisdictional claims in published maps and institutional affiliations.

References

- Sabo Y, Walsh D, Barry DS, Tinaztepe S, de Los Santos K, Goff SP, et al. HIV-1 induces the formation of stable microtubules to enhance early infection. *Cell Host Microbe*. 2013;14:535–46.
- Delaney MK, Malikov V, Chai Q, Zhao G, Naghavi MH. Distinct functions of diaphanous-related formins regulate HIV-1 uncoating and transport. *Proc Natl Acad Sci USA*. 2017;114: E6932–41.
- Dharan A, Campbell EM. Role of microtubules and microtubule-associated proteins in HIV-1 infection. *J Virol*. 2018;92:e00085–18.
- Andersen RO, Turnbull DW, Johnson EA, Doe CQ. Sgt1 acts via an LKB1/AMPK pathway to establish cortical polarity in larval neuroblasts. *Dev Biol*. 2012;363:258–65.
- Davies AE, Kaplan KB. Hsp90-Sgt1 and Skp1 target human Mis12 complexes to ensure efficient formation of kinetochore-microtubule binding sites. *J Cell Biol*. 2010;189:261–74.
- Kitagawa K, Skowrya D, Elledge SJ, Harper JW, Hieter P. SGT1 encodes an essential component of the yeast kinetochore assembly pathway and a novel subunit of the SCF ubiquitin ligase complex. *Mol Cell*. 1999;4:21–33.
- Liu W, Evanoff DP, Chen X, Luo Y. Urinary bladder epithelium antigen induces CD8+ T cell tolerance, activation, and autoimmune response. *J Immunol*. 2007;178:539–46.
- Steensgaard P, Garre M, Muradore I, Transidico P, Nigg EA, Kitagawa K, et al. Sgt1 is required for human kinetochore assembly. *EMBO Rep*. 2004;5:626–31.
- Mayor A, Martinon F, De Smedt T, Petrilli V, Tschopp J. A crucial function of SGT1 and HSP90 in inflammasome activity links mammalian and plant innate immune responses. *Nat Immunol*. 2007;8:497–503.
- Allouch A, David A, Amie SM, Lahouassa H, Chartier L, Margottin-Goguet F, et al. p21-mediated RNR2 repression restricts HIV-1 replication in macrophages by inhibiting dNTP biosynthesis pathway. *Proc Natl Acad Sci USA*. 2013;110: E3997–4006.
- Di Primio C, Quercioli V, Allouch A, Gijbsers R, Christ F, Debyser Z, et al. Single-cell imaging of HIV-1 provirus (SCIP). *Proc Natl Acad Sci USA*. 2013;110:5636–41.
- Francis AC, Di Primio C, Quercioli V, Valentini P, Boll A, Girelli G, et al. Second generation imaging of nuclear/cytoplasmic HIV-1 complexes. *AIDS Res Hum Retroviruses*. 2014;30:717–26.
- Delelis O, Malet I, Na L, Tchertanov L, Calvez V, Marcelin AG, et al. The G140S mutation in HIV integrases from raltegravir-resistant patients rescues catalytic defect due to the resistance Q148H mutation. *Nucleic Acids Res*. 2009;37:1193–201.
- David A, Saez-Cirion A, Versmisse P, Malbec O, Iannascoli B, Herschke F, et al. The engagement of activating FcgammaRs inhibits primate lentivirus replication in human macrophages. *J Immunol*. 2006;177:6291–300.
- McDonald D, Vodicka MA, Lucero G, Svitkina TM, Borisy GG, Emerman M, et al. Visualization of the intracellular behavior of HIV in living cells. *J Cell Biol*. 2002;159:441–52.
- Dunn KW, Kamocka MM, McDonald JH. A practical guide to evaluating colocalization in biological microscopy. *Am J Physiol Cell Physiol*. 2011;300:C723–42.
- Svarovskaia ES, Barr R, Zhang X, Pais GC, Marchand C, Pommier Y, et al. Azido-containing diketo acid derivatives inhibit human immunodeficiency virus type 1 integrase *in vivo* and influence the frequency of deletions at two-long-terminal-repeat-circle junctions. *J Virol*. 2004;78:3210–22.
- Devroe E, Engelman A, Silver PA. Intracellular transport of human immunodeficiency virus type 1 integrase. *J Cell Sci*. 2003;116:4401–8.

19. Akhmanova A, Steinmetz MO. Control of microtubule organization and dynamics: two ends in the limelight. *Nat Rev Mol Cell Biol.* 2015;16:711–26.
20. Bieling P, Kandels-Lewis S, Telley IA, van Dijk J, Janke C, Surrey T. CLIP-170 tracks growing microtubule ends by dynamically recognizing composite EB1/tubulin-binding sites. *J Cell Biol.* 2008;183:1223–33.
21. Matov A, Applegate K, Kumar P, Thoma C, Krek W, Danuser G, et al. Analysis of microtubule dynamic instability using a plus-end growth marker. *Nat Methods.* 2017;7:761–8.
22. Seetapun D, Castle BT, McIntyre AJ, Tran PT, Odde DJ. Estimating the microtubule GTP cap size in vivo. *Curr Biol.* 2012;22:1681–7.
23. Albanese A, Arosio D, Terreni M, Cereseto A. HIV-1 pre-integration complexes selectively target decondensed chromatin in the nuclear periphery. *PLoS One.* 2008;3:e2413.
24. Fernandez J, Portilho DM, Danckaert A, Munier S, Becker A, Roux P, et al. Microtubule-associated proteins 1 (MAP1) promote human immunodeficiency virus type I (HIV-1) intracytoplasmic routing to the nucleus. *J Biol Chem.* 2015;290:4631–46.
25. Francis AC, Melikyan GB. Single HIV-1 imaging reveals progression of infection through CA-dependent steps of docking at the nuclear pore, uncoating, and nuclear transport. *Cell Host Microbe.* 2018;23:536–48.e6.
26. Desfarges S, Salin B, Calmels C, Andreola ML, Parissi V, Fournier M. HIV-1 integrase trafficking in *S. cerevisiae*: a useful model to dissect the microtubule network involvement of viral protein nuclear import. *Yeast.* 2009;26:39–54.
27. de Soultrait VR, Caumont A, Durrens P, Calmels C, Parissi V, Recordon P, et al. HIV-1 integrase interacts with yeast microtubule-associated proteins. *Biochim Biophys Acta.* 2002;1575:40–8.

Affiliations

Awatef Allouch^{1,2,3,4} · **Cristina Di Primio**⁵ · **Audrey Paoletti**^{1,2,3,4} · **Gabrielle Lê-Bury**^{6,7,8} · **Frédéric Subra**⁹ · **Valentina Quercioli**⁵ · **Roberta Nardacci**¹⁰ · **Annie David**¹¹ · **Héla Saïdi**¹² · **Anna Cereseto**¹³ · **David M. Ojcius** ^{14,15} · **Guillaume Montagnac**¹⁶ · **Florence Niedergang**^{6,7,8} · **Gianfranco Pancino**¹¹ · **Asier Saez-Cirion** ¹¹ · **Mauro Piacentini**^{10,17} · **Marie-Lise Gougeon**¹² · **Guido Kroemer**^{8,18,19,20,21,22} · **Jean-Luc Perfettini** ^{1,2,3,4,14}

¹ Cell Death and Aging Team, Gustave Roussy Cancer Campus, F-94805 Villejuif, France

² Laboratory of Molecular Radiotherapy, INSERM U1030, Gustave Roussy Cancer Campus, F-94805 Villejuif, France

³ Gustave Roussy Cancer Campus, F-94805 Villejuif, France

⁴ Université Paris-Saclay, 114 Rue Edouard Vaillant, F-94805 Villejuif, France

⁵ Bio@SNS Laboratory, Scuola Normale Superiore, Piazza dei Cavalieri 7, 56126 Pisa, Italy

⁶ INSERM U1016, Institut Cochin, F-75013 Paris, France

⁷ CNRS, UMR 8104, F-75013 Paris, France

⁸ Université Paris Descartes, Université de Paris, F-75006 Paris, France

⁹ CNRS UMR 8113 LBPA, Ecole Normale Supérieure de Cachan, 61 Avenue du Président Wilson, F-94230 Cachan, France

¹⁰ National Institute for Infectious Diseases “Lazzaro Spallanzani”, Via Portuense 292, I-00149 Rome, Italy

¹¹ Unité HIV, inflammation and Persistence, 28 Rue du Dr Roux, F-75015 Paris, France

¹² Antiviral Immunity, Biotherapy and Vaccine Unit, Institut Pasteur, 25 Rue du Dr Roux, F-75015 Paris, France

¹³ Laboratory of Molecular Virology, Centre for Integrative Biology, University of Trento, Via Sommarive 9, Povo, I-38123 Trento, Italy

¹⁴ Department of Biomedical Sciences, Arthur Dugoni School of Dentistry, University of the Pacific, San Francisco, CA 94103, USA

¹⁵ Université de Paris, F-75013 Paris, France

¹⁶ INSERM U1170, Gustave Roussy Cancer Campus, F-94805 Villejuif, France

¹⁷ Department of Biology, University of Rome “Tor Vergata”, Via della Ricerca Scientifica 1, I-00173 Rome, Italy

¹⁸ INSERM U848, Gustave Roussy Cancer Campus, F-94805 Villejuif, France

¹⁹ Metabolomics Platform, Gustave Roussy Cancer Campus, F-94805 Villejuif, France

²⁰ Equipe 11 Labellisée Ligue Contre le Cancer, Centre de Recherche des Cordeliers, INSERM U1138, F-75006 Paris, France

²¹ Pôle de Biologie, Hôpital Européen Georges-Pompidou, AP-HP, F-75015 Paris, France

²² Department of Women’s and Children’s Health, Karolinska Institute, Karolinska University Hospital, S-17176 Stockholm, Sweden